Optimization of the aeration strategies in a deammonification sequencing batch reactor for efficient nitrogen removal and mitigation of N2O production

Journal:	*Environmental Science & Technology*
Manuscript ID	es-2020-042297.R2
Manuscript Type:	Article
Date Submitted by the Author:	14-Dec-2020
Complete List of Authors:	Alhazmi, hussein; Gdańsk University of Technology, Faculty of Civil and Environmental Engineering Lu, Xi; Gdańsk University of Technology, Faculty of Civil and Environmental Engineering; Tongji University, Institute of Environmental Science and Engineering Majtacz, Joanna; Gdańsk University of Technology, Faculty of Civil and Environmental Engineering Kowal, Przemysław ; Gdańsk University of Technology Faculty of Civil and Environmental Engineering, Sanitary Engineering Xie, Li; Tongji University, Institute of Environmental Science and Engineering Makinia, Jacek; Gdańsk University of Technology, Faculty of Civil and Environmental Engineering

Optimization of the aeration strategies in a deammonification sequencing batch reactor for efficient nitrogen removal and mitigation of N_2O production

Hussein E. Al-Hazmi[a], Xi Lu[a,b], Joanna Majtacz[a], Przemyslaw Kowal[a], Li Xie[b], Jacek Makinia[a]*

[a] Faculty of Civil and Environmental Engineering, Gdansk University of Technology, ul. Narutowicza 11/12, 80-233, Gdansk, Poland

[b] Institute of Environmental Science and Engineering, Tongji University, 1239 Siping Road, Shanghai, 200092, China

KEYWORDS. Aeration control; Anammox; Granular sludge; Mathematical modelling; Nitrous oxide production

ABSTRACT. In deammonification systems, nitrite-oxidizing bacteria (NOB) suppression and nitrous oxide (N_2O) mitigation are two important operational objectives. To carry out this multivariable analysis of response, a comprehensive model for the N cycle was developed and evaluated against experimental data from a

laboratory-scale deammonification granular sludge sequencing batch reactor. Different aeration strategies were tested and the manipulated variables comprised the dissolved oxygen (DO) set point in the aerated phase, aeration on/off frequency (F) and the ratio (R) between the non-aerated and aerated phase durations. Experimental results showed that a high ammonium utilization rate (AUR) in relation to the low nitrate production rate (NPR) (NPR/AUR = 0.07-0.08) and limited N_2O emissions (E_{N2O} < 2%) could be achieved at the DO set point = 0.7 mg O_2/L, R ratio = 2 and F frequency = 6-7 h^{-1}. Under specific operational conditions (biomass concentration, NH_4^+-N loading rate and temperature), simulation results confirmed the feasible aeration strategies for the trade-offs between the NOB suppression and N_2O emission. The intermittent aeration regimes led to frequent shifts in the predominating N_2O production pathways, i.e. hydroxylamine (NH_2OH) oxidation (aerated phase) vs. autotrophic denitrification (non-aerated phase). The inclusion of the extracellular polymeric substances mechanism in the model explained the observed activity of heterotrophs, especially *Anaerolineae*, and granule formation.

1. INTRODUCTION

Deammonification is an effective and energy efficient process for nitrogen removal in wastewater treatment plants (WWTPs). The process can be performed in many configurations by two functional microorganisms, including ammonia oxidizing

bacteria (AOB) and anaerobic ammonia oxidation (anammox) bacteria. Those microorganisms coexist and interact with heterotrophs and nitrite oxidizing bacteria (NOB). In particular, the activity of NOB should be suppressed due to the competition for either dissolved oxygen (DO) (with AOB) or nitrite (NO_2^--N) (with anammox bacteria). Among different methods proposed for NOB suppression [1–3], tight DO control is regarded as the most effective approach [4,5].

Sequencing batch reactors (SBRs) with granular sludge are common deammonification systems, in which the DO set point and aeration mode (continuous vs. intermittent) are important control variables. The intermittent aeration mode is controlled by two manipulated variables, including the aeration on/off frequency (F), representing the number of the aeration phases per hour, and the ratio (R) between the non-aerated and aerated phase durations. The intermittent aeration allows to outcompete NOB by AOB due to a lag phase necessary for NOB to respond to the transition from anoxic to aerobic conditions or potential inhibition of NOB by the intermediate product, i.e. hydroxylamine (NH_2OH) [6]. In order to enhance NOB suppression, the intermittent aeration with either high DO set points [7] or lower DO set points [3] has been proposed. Cao et al. [1] provided the following explanation for this apparent inconsistency. Under high DO levels (>1.5 mg O_2/L), the growth rate of r-strategists *Nitrosomonas*-AOB is higher than that of r-strategists *Nitrobacter*-NOB. On the contrary, lower DO levels (<1.0 mg O_2/L) may favor *Nitrosomonas*-AOB and

partially suppress NOB by selecting only K-strategists NOB (*Nitrospira)* rather than r-strategists NOB (*Nitrobacter)*.

An optimized intermittent aeration strategy may also comprise a higher aeration on/off frequency [8], which could be beneficial for both NOB suppression and reduction of energy consumption [9]. However, under DO-limited and nitrite-elevated conditions, the sustainability of deammonification systems may be questioned due to a potentially significant nitrous oxide (N_2O) production [10]. Simultaneous high nitrogen removal efficiency and low N_2O production depend on many factors, e.g. wastewater composition, granule size, the presence of organic substrates, nitrogen loading rate, aeration pattern, pH and temperature [11–14]. Moreover, an appropriate aeration control may also minimize N_2O production in deammonification systems [11,15,16]. However, no specific operational strategy has been proposed yet for improving nitrogen removal performance while simultaneously mitigating N_2O production [13,17].

A few model-based studies have illustrated the effects of aeration patterns on specific aspects of the nitrogen cycle, including either NOB suppression [18,19] or N_2O mitigation in deammonification systems [13]. However, no models have been applied to carry out a multivariable analysis of response in those systems for efficient nitrogen removal performance, NOB suppression and mitigation of N_2O production. It should be noted that in the case of granular deammonification systems, selection of a conceptual model becomes important. Basically, there are two different (but numerically equivalent) approaches, including biofilm models and “apparent kinetics”

[20]. The advantage of the latter approach is that typical monitoring data can be used for model calibration [21].

In this study, a comprehensive model for the N cycle was developed and evaluated against comprehensive experimental data from a laboratory-scale deammonification granular system. Subsequently, the model was used as a tool for the understanding and integrated optimization of deammonification systems (process performance vs. sustainability). The model-based analysis was supported by microbiological investigations with the 16S rDNA Illumina High-Throughput Sequencing to identify microorganisms present in the studied system. The main innovation and contribution of this study is the multivariate analysis of BNR performance, NOB suppression and N_2O mitigation by manipulating the DO set point and intermittent aeration control settings (durations and proportions of on/off periods).

2. MATERIALS AND METHODS

2.1. Laboratory setup and monitoring. A bench-scale SBR with a working volume of 10 L was inoculated with biomass originated from a full-scale sidestream deammonification SBR system in Plettenberg (Germany) [22]. The detailed description of laboratory setup and monitoring (including liquid N_2O concentrations) can be found in the Supporting Information (SI, Section S.1).

2.2. Experimental design and data collection. Over the entire cultivation period of 314 days, three series of experiments (test trials) were carried out under various

operational conditions (scenarios) in terms of the aeration pattern, biomass concentration, hydraulic retention time (HRT) and NH_4^+-N loading rate (NLR) (Table 1). In test trial no. 1, a continuous aeration pattern (scenario 1) was compared with three intermittent aeration patterns (scenarios 2-4). In the latter scenarios, different DO set points, F frequencies and R ratios were used (Table 1). Subsequently, four different R ratios were evaluated in test trial no. 2 with the doubled biomass concentration (scenarios 5-8). Next, a higher F frequency was tested under different R ratios in test trial no. 3 (scenarios 9-14) with the biomass concentration increased fourfold in comparison with test trial no. 1. The length of a single operational cycle of the studied SBR was variable (5-24 h) and the cycle in each scenario consisted of four phases as described in the footnote to Table 1. The stable operation was reached between each test trial and a fixed number of cycles were considered in each scenario (Table 1). During the experiments, mixed liquor samples were withdrawn in the reaction phase every 30 min (scenario 1), 15-45 min (scenarios 2-3), 2 h (scenarios 4 and 9-14), and 6 h (scenarios 5-8). The samples were immediately filtered through 1.2 μm pore-size nitrocellulose membrane filters (Whatman, Kent, UK) under vacuum pressure and analyzed for ammonium (NH_4^+-N), nitrate (NO_3^--N), and nitrite (NO_2^--N) concentrations. The detailed description of the analytical methods can be found in the SI (section S.2).

119 **Table 1.** Summary of the operational conditions (aeration pattern, biomass concentration, HRT and NLR) in the studied SBR during

120 the entire cultivation period

Days	Modeling phase	Test trial no.	Scenario no.	Aeration on/off (min)	R ratio	F frequency	DO set point (mg O$_2$/L)	HRT (d)	Number of cycles	Influent NH_4^+-N (mg N/L)	NLR (mg N/(L·d))	MLVSS/ MLSS (mg/L)	Test objectives
1-4	Calibration	1*	1	Continuous	-	-	0.3	0.83	4	528 ± 121	634 ± 145	993 ± 184/ 1530 ± 42	Continuous aeration vs. different intermittent aeration patterns. Moderate NH_4^+-N load and low biomass concentration
			2	15/45	3	1.0	1.0		4				
			3	15/45	3	1.0	0.5		4				
			4	8/22	2.7	2.0	0.5		4				
5-154	Stable operation*			8/22	2.7	2.0	0.5	0.83		528 ± 121	634 ± 145	-	150 days of stable operation
155-158	Recalibration	2**	5	5/10	2	4.0	0.7	2.5	1	846 ± 46	339 ± 18	2054 ± 76/ 2481 ± 114	Intermittent aeration with a different length of the non-aerated phase following the aerated phase. High NH_4^+-N load and moderate biomass concentration
			6	5/15	3	3.0			1				
			7	5/20	4	2.4			1				
			8	5/25	5	2.0			1				
159-	Stable operation**			5/20	4	2.4	0.7	2.5		846 ± 46	339 ± 18	-	150 days of stable operation
309-314	Validation	3***	9	5/5	1	6.0	0.7	0.83	3	846 ± 46	1016 ± 55	3850 ±235/ 5847 ± 173	Intermittent aeration with higher aeration frequency. High NH_4^+-N load and high biomass concentration
			10	5/10	2	4.0			3				
			11	5/15	3	3.0			3				
			12	3/3	1	10.0			3				
			13	3/6	2	6.7			3				

	14	3/9	3	5.0	3	

Note:

* total operational cycle of 5 h, including 4 phases, i.e. 30 min of feeding (2.5 L), 4 h of reaction, 10 min of sedimentation and 20 min of decantation (2.5 L).

** total operational cycle of 24 h, including 4 phases, i.e. 30 min of feeding (4 L), 23 h of reaction, 2 min of sedimentation and 28 min of decantation (4 L).

*** total operational cycle of 8 h, including 4 phases, i.e. 30 min of feeding (4 L), 7 h of reaction, 3 min of sedimentation and 27 min of decantation (4 L)

129

130 **2.3. Process performance indicators.** The efficiency of nitrogen removal and N_2O
131 emission were used as indicators to compare process performance of the analyzed
132 scenarios. With respect to the first indicator, the AOB and NOB activities were
133 measured by the specific rates of ammonium utilization (AUR, mg N/(g VSS·h)) and
134 nitrate production (NPR, mg N/(g VSS·h)), respectively. The NPR/AUR ratio was
135 assumed to represent the normalized NOB activity in comparison with the AOB
136 activity. However, it should be emphasized that both rates could in practice be
137 influenced by the activities of other microorganisms, i.e. heterotrophs (NPR) and
138 anammox bacteria (NPR and AUR).

139 With respect to the second indicator, the N_2O emission factor (E_{N2O} (%)) may be
140 normalized with either amount of treated wastewater, PE year, N load removed or
141 influent N load. In this study, the latter approach was assumed and E_{N2O} was
142 calculated by dividing the mass of N_2O emitted (M_{N2O} (mg N/(L·d))) by the NLR (mg
143 N/(L·d)) (Eq. 1):

144 $$E_{N2O} = \frac{M_{N2O}}{NLR} \cdot 100\% \quad (1)$$

145 The mass M_{N2O} (mg N/(L·d)) was calculated by integrating the N_2O stripping rates
146 (r_{N_2O} (mg N/(L·d))) over the unit time (dt (d)) and dividing by the overall reaction time
147 (t (d)) (Eq. 2):

148 $$M_{N2O} = \frac{\int r_{N_2O} \cdot dt}{t} \quad (2)$$

149 The rate r_{N_2O} (mg N/(L·d)) consists of two components related to aerated and non-
150 aerated conditions. The details of r_{N_2O} calculations can be found elsewhere [23].

151 **2.4. Microbial examination.** *2.4.1. DNA extraction.* The microbial community
152 structure in the studied SBR was examined during each modelling phase, including
153 the calibration phase (CAL), recalibration phase (REC) after 150 days of cultivation,
154 and during the validation phase (VAL) after 300 days of cultivation. The samples were
155 withdrawn from the reactor and transferred into a 15 ml DNase-free tube. The
156 supernatant was removed and the tube was filled with biomass twice to thicken the
157 sludge concentration. The samples were stored at −25°C prior to DNA extraction. For the
158 DNA extraction, the sludge sample was initially centrifuged at 10000 g for 10 min and
159 washed with phosphate buffer. The centrifugation process was repeated and 200 mg
160 of the pellet of the sample was collected for the DNA extraction reaction, which was
161 carried out using the FastDNA™ SPIN KIT (MP Biomedicals, USA) following the
162 manufacturer's manual. DNA acquired from purification was used for the Illumina Next
163 Generation Sequencing protocol.

164 *2.4.2. High-throughput DNA sequencing.* High-throughput Illumina sequencing
165 targeting the V3-V4 region of the 16S rRNA gene was performed with S-d-Bact-0341-
166 b-S-17 and S-d-Bact-0785-a-A-21 primers [24] and NEBNext®High-Fidelity 2X PCR
167 Master Mix (Bio Labs inc., USA) following the manufacturer's manual. The detailed
168 Illumina Next Generation Sequencing protocol can be found in the SI (section S.3).
169 Taxonomic differences between the metagenomes were analyzed using Statistical

Analysis of Metagenomic Profiles (STAMP v. 2.1.3) [25] and visualized as heatmaps. A genetic distance between the samples was tested by the ANOVA test, followed by the post-hoc Tukey-Kramer test at 0.95 significance, and visualized as a dendrogram built up with the unweighted pair group method with the arithmetic mean algorithm (UPGMA). The data sets were uploaded to the MetaGenome Rapid Annotation Subsystems Technology (MG-RAST) to enable public access to the files under the accession numbers: mgm4784320.3 (CAL), mgm4784321.3 (REC) and mgm4898872.3 (VAL).

2.5. Modelling approach. *2.5.1. Model development.* A conceptual model of the biochemical transformations in the studied SBR is shown in Figure 1. The N_2O production/consumption mechanisms (along with the gas-liquid transfer) were adopted from Zaborowska et al. [23], including NH_2OH oxidation (NN) and autotrophic denitrification (ND) mediated by AOB and three-step heterotrophic denitrification (HD) with NO_2^--N and N_2O as intermediates. For modeling, the only source of electron donors for autotrophic denitrification was NH_4^+-N [26]. Due to the high abundance of heterotrophic biomass (42-68%) present in the studied system fed only with inorganic substrates, the heterotrophic growth was also considered in the model. It has earlier been reported that extracellular polymeric substances (EPS) and soluble microbial products (SMP) could play a vital role in heterotrophic growth in anammox biofilm systems [27,28]. However, only one study investigated the effect of heterotrophic growth on autotrophic nitrogen removal in granular systems [29], without considering the new

kinetics of microbial products formation from anammox. In the present study, the model incorporated heterotrophic growth on (i) readily biodegradable substrate (S_S) produced from the biomass decay, and (ii) SMPs, specifically biomass associated products (S_{BAP}) and utilization associated products (S_{UAP}). With respect to formation of SMPs, the following assumptions were made:

- S_{UAP} was formed during growth of autotrophs (AOB, NOB) [27], and autotrophs (anammox) and heterotrophs on S_S [28].
- S_{BAP} was produced from X_{EPS} hydrolysis and biomass decay [28].

The extended model was implemented in GPS-X 8.0 simulation platform (Hydromantis, Canada), using a special utility called "Model Developer", based on the standard notation (Petersen-Gujer matrix) of ASM1 [30]. Further details regarding the model development can be found in the SI (Section S.4), including the definition of the state variables, stoichiometric matrix, process rate equations, and kinetic and stoichiometric parameters (Tables S1-S4).

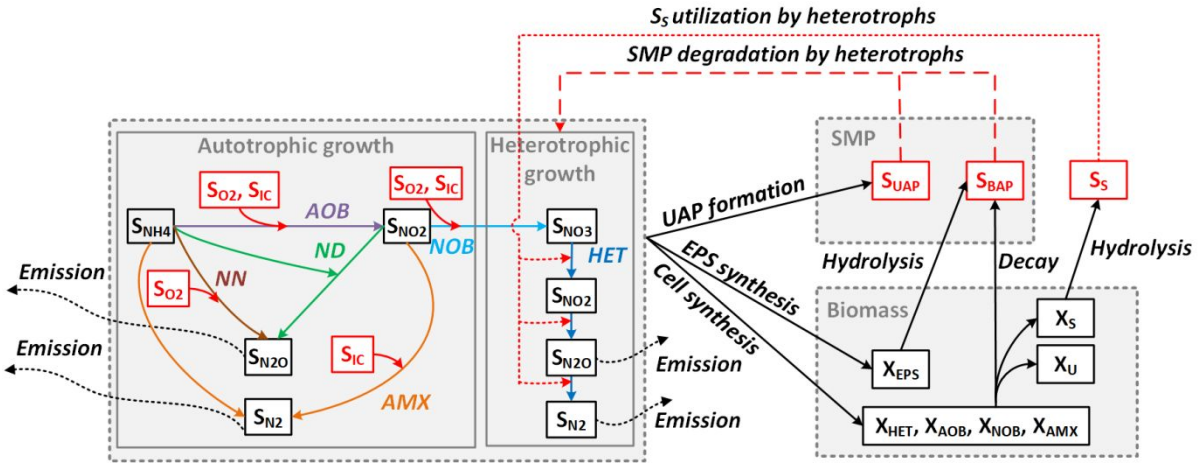

Figure 1. The conceptual model of biochemical transformations in the studied SBR (fed only with inorganic substrates) ("S_{NO2}", "S_{N2O}" and "S_{N2}" for autotrophs and heterotrophs could simultaneously be used by both groups of microorganisms).

2.5.2. Model layout and initial biomass composition. The GPS-X model layout consisted of an SBR with a wastewater influent object. Because the interest of the study was focused on the liquid phase concentrations, the granular sludge was modelled using the "apparent" kinetics approach [20,21]. The aeration patterns were controlled by setting the DO set point on/off periods in "Timer Controller" and manipulated by adjusting the PI control module (controller sampling time = 20 s; proportional gain = 500; integral time = 0.0001 d). The DO controller manipulated the field oxygen mass transfer coefficient (K_La) directly to match the desired DO set point and calculated the airflow rate. Typical examples of the predicted and measured DO concentrations are shown in Figure S1. The N_2O emission during the aerated phase (air-stripping) was influenced by the K_La coefficient and estimated airflow rate [23]. The initial active biomass composition in each modelling phase (CAL, REC and VAL) was assumed based on the results of the metagenomics analysis (Table S5). The share of the remaining bacteria, either unclassified or other, were 31.1% (CAL), 45.7% (REC), 41.1% (VAL) (Table S5). These bacteria, not supposed to be responsible for the considered biochemical reactions, were incorporated in the model as the slowly biodegradable substrate (X_S, 92% of the remaining biomass) and unbiodegradable particulates from cell decay (X_U, 8% of the remaining biomass). That assumption was

made based on the typical decay stoichiometry of biomass in the ASM1 [30]. The SMP mechanisms were investigated assuming the initial SMP ($S_{UAP,}$ S_{BAP}) and EPS (X_{EPS}) concentrations to be 0 mg COD/L and 0%, respectively.

2.5.3. Model calibration and validation. Figure S2 shows the four-step protocol of model calibration and validation with the data from test trials no. 1-3, including preliminary simulation, model calibration, recalibration, and validation. The detailed description of these steps can be found in the SI (Section S.5). The conversion rates of COD and N compounds were calculated in the model and visualized in the Sankey graphs. A more advanced uncertainty analysis of N_2O production in the studied system, based on the combination of global sensitivity analysis and Generalized Likelihood Uncertainty Estimation methodology, can be found elsewhere [31].

2.5.4. Model-based optimization of intermittent aeration strategies. In order to simultaneously maximize the nitrogen removal performance and minimize N_2O emissions in the deammonification SBR, different intermittent aeration strategies were analyzed with the validated model at a high biomass concentration (MLVSS ≈ 4000 mg/L) (test trial no. 3). The three operating parameters of interest, including the DO set point in the aerated phase, F frequency, and R ratio were manipulated within the following ranges: DO = 0.3-2.1 mg O_2/L (interval of 0.2 mg O_2/L), F = 0.5-10 h^{-1} (interval of 0.5 h^{-1}), and R = 0.5-5.0 (interval of 0.5). Altogether, 2000 automatic simulation runs were carried out by executing Python 3.7 scripts within the GPS-X interface. The 2D-response contour plots of the three operational parameters on the

AOB activity, NOB activity and N_2O emissions were generated in MATLAB R2019b (The MathWorks, Inc., USA). The feasible parameter ranges were scattered in the red region, including all the red scatters when the AUR > 12 mg N/(g VSS·h), NPR/AUR < 0.1 and E_{N2O} < 2%.

2.5.5. Model limitations. Limitations to the applications. The model structure is applicable to the systems treating real wastewater (reject water) without any further modifications or extensions, but model calibration/validation would be required for each specific case. As a consequence, the regions of the optimal aeration settings may also change.

Limitations to the optimization of operational parameters. The aeration strategy was analyzed under specific operational conditions in terms of three manipulated variables, including the DO set point, F frequency and R ratio. However, the region of the optimal aeration settings may change while considering other operational parameters, such as the biomass concentration, NH_4^+-N loading rate and temperature.

Limitations to the apparent kinetics. The “apparent kinetics” approach was used as a model concept for granular sludge in the studied SBR. However, due to the specific characteristics of the granules (e.g. size distribution, density, porosity, etc.), the results of the present study may not be directly applicable to other systems. For example, in a continuously aerated system, the process rate of anammox bacteria would be strongly suppressed, which requires different kinetic parameters or higher concentrations of anammox bacteria compared to a biofilm model.

Limitations to describe alkalinity and pH. As the pH was controlled in the studied reactor, alkalinity was not considered in the developed model. The model can be extended with alkalinity as a state variable when low pH conditions may occur. The details of considering alkalinity in biokinetic models were described by Henze et al. [30].

Limitations to describe the lag phase for NOB. The effect of the lag phase for NOB to respond the transition from anoxic to aerobic conditions was only reflected in lower DO affinities of NOB in comparison with AOB[32].

Limitations to describe autotrophic denitrification by AOB. Since NH_2OH oxidation was not specifically considered in the model, it was assumed that the overall NH_4^+-N oxidation to NO_2^--N would transfer electrons to the internally stored AOB electron pool. Those electrons could subsequently be used for AOB-mediated reduction of NO_2^--N to N_2O-N. Therefore, a prerequisite for that process would be a preceding aerobic phase or continuous low-DO conditions [33]. Under prolonged anoxic conditions, autotrophic denitrification by AOB could be stopped due to exhausting electrons from the pool. That phenomenon could not be predicted as the transfer of electrons was not considered in the model.

Limitations to the calibration protocol. Due to the limitation of the simulation platform (GPS-X), the selected scenarios could not be calibrated simultaneously with the same parameter set (i.e. the objective function taking both scenarios into account simultaneously). Alternatively, the use of the mean value of the estimated parameters was applied only when both scenarios were carefully calibrated with similar parameter

values. It was implicitly assumed that the model response to the parameters was linear, after taking into consideration the different biomass compositions and concentrations at each stage (CAL, REC and VAL). However, the selected approach sacrificed the model accuracy for a faster calibration.

3. RESULTS AND DISCUSSION

3.1. Nitrogen removal performance and N_2O production under different aeration conditions.

The process performance indicators of the studied SBR are summarized in Table S6, whereas the dynamic behavior of DO and inorganic nitrogen compounds (N_2O-N, NH_4^+-N, NO_3^--N, NO_2^--N) in the three trials are shown in Figures 2-4.

In test trial no. 1 with the moderate NH_4^+-N load and low biomass concentration, continuous aeration at the low DO set point (0.3 mg O_2/L) (scenario 1) apparently favored the activity of AOB, which was reflected by the high AUR, but also insufficiently suppressed NOB (NPR/AUR = 0.66). The switch to the intermittent aeration mode (scenarios 2-3) explicitly improved the efficiency of nitrogen removal, primarily due to suppressing NOB (NPR/AUR = 0.25-0.33), but considerably increased the liquid N_2O concentrations. Further increasing the F frequency (scenario 4) indicated better suppression of NOB activity and N_2O production while maintaining the AOB activity.

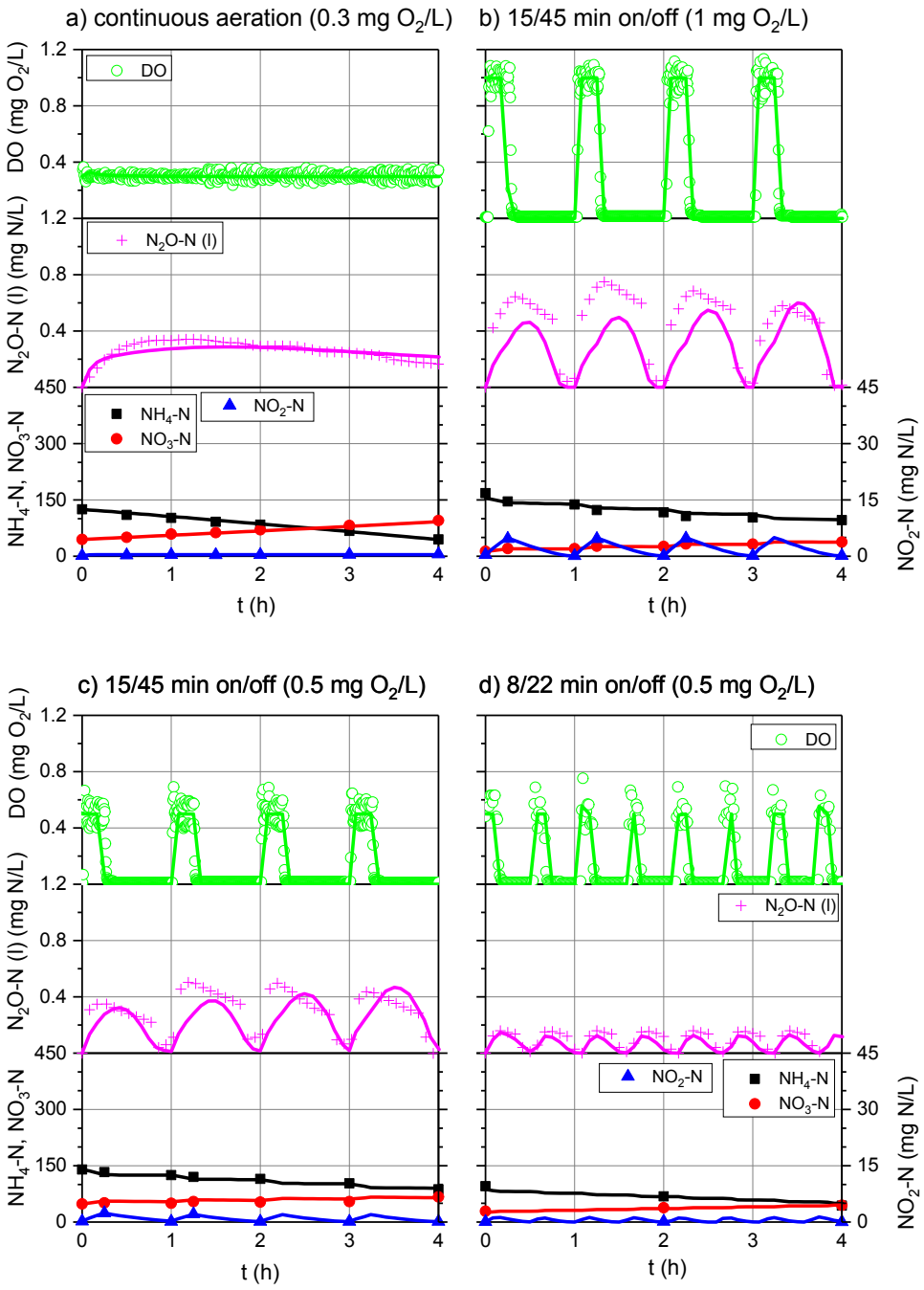

Figure 2. Measured data (scatters) vs. model predictions (solid lines) of DO and inorganic nitrogen compounds (N_2O-N, NH_4^+-N, NO_3^--N, NO_2^--N) in test trial no. 1: (a) continuous aeration at DO = 0.3 mg O_2/L (SCE1), (b) intermittent aeration 15/45 min on/off at DO = 1.0 mg O_2/L (when on) (SCE2), (c) intermittent aeration 15/45 min on/off

315 at DO = 0.5 mg O_2/L (when on) (SCE3), (d) intermittent aeration 8/22 min on/off at DO
316 = 0.5 mg O_2/L (when on) (SCE4).

317 Test trial no. 2 was carried out after 150 d of cultivation, at a higher biomass
318 concentration (MLVSS ≈ 2000 mg/L) and constant DO set point of 0.7 mg O_2/L (Figure
319 3). The increasing R ratios from 2 to 4 (scenarios 5-7) resulted in the improved NOB
320 suppression (NPR/AUR = 0.16-0.09) without compromising the AOB activity (AUR =
321 7.4-9.0 mg N/(g VSS·h)). Furthermore, the liquid N_2O concentrations and N_2O
322 emission factors decreased due to enhanced anammox activities in the anoxic periods
323 and reduced NO_2^--N accumulation (from 35 to 5 mg N/L) during the whole period. The
324 extension of the non-aerated phase up to 25 min at R = 5 (scenario 8) allowed to
325 mitigate the N_2O production, while maintaining the favorable NPR/AUR ratio (= 0.09).
326 However, the overall process performance deteriorated due to the decreased AUR.

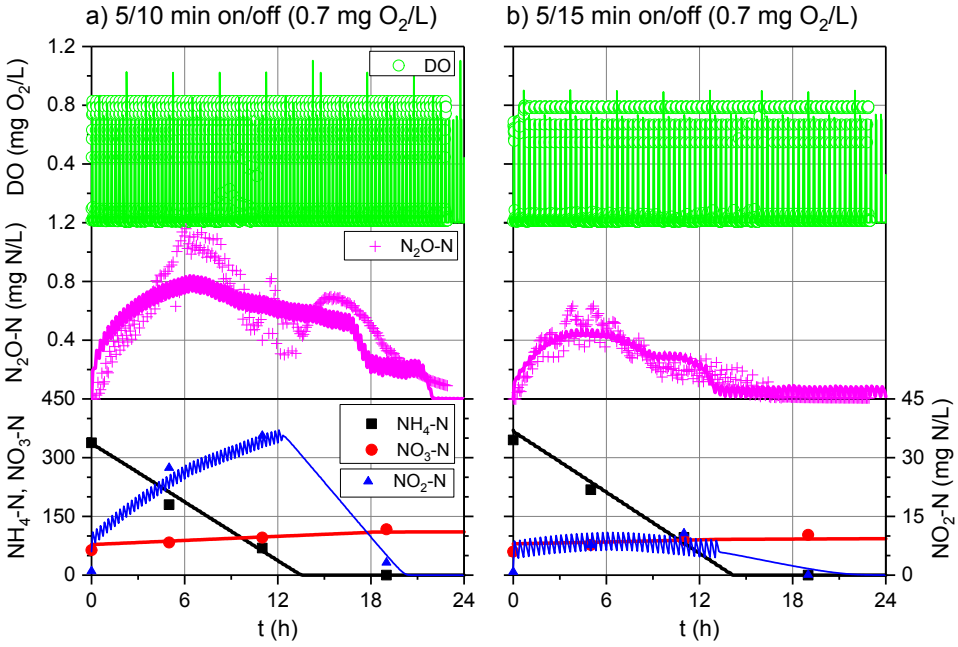

327

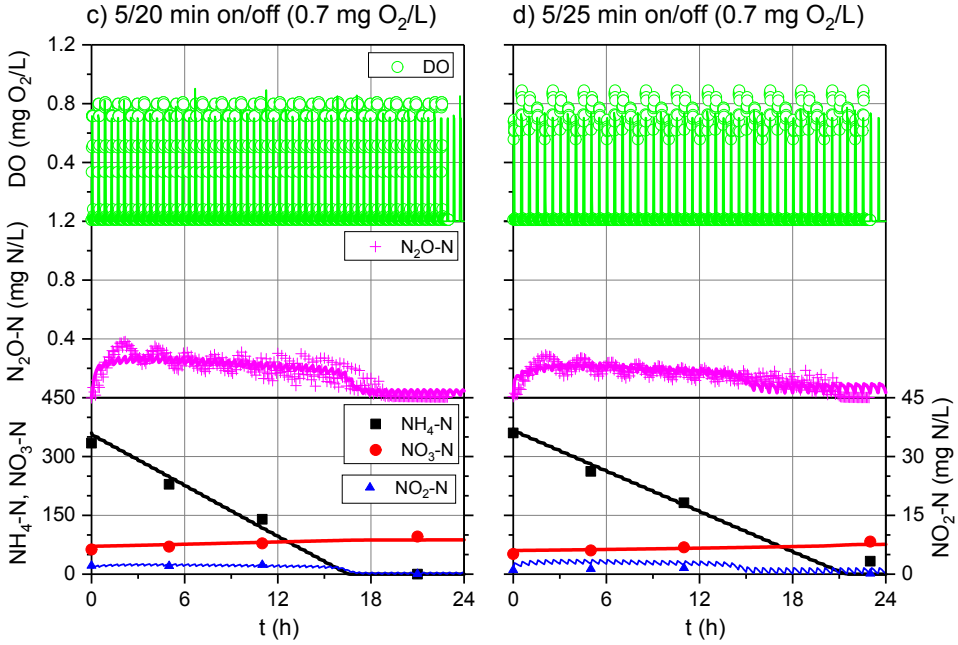

328

329 **Figure 3**. Measured data (scatters) vs. model predictions (solid lines) of DO and
330 inorganic nitrogen compounds (N_2O-N, NH_4^+-N, NO_3^--N, NO_2^--N) in test trial no. 2: (a)
331 intermittent aeration 5/10 min on/off at DO = 0.7 mg O_2/L (when on) (SCE5), (b)
332 intermittent aeration 5/15 min on/off at DO = 0.7 mg O_2/L (when on) (SCE6), (c)
333 intermittent aeration 5/20 min on/off at DO = 0.7 mg O_2/L (when on) (SCE7), (d)
334 intermittent aeration 5/25 min on/off at DO = 0.7 mg O_2/L (when on) (SCE8).

335 The final test trial no. 3 was carried out after over 300 days of cultivation, when the
336 MLVSS reached approximately 4000 mg/L (Figure 4). The DO set point was kept
337 constant at 0.7 mg O_2/L and that trial focused on investigating the effect of aeration
338 on/off frequencies at the R ratios ranging from 1 to 3. In all the scenarios, the
339 NPR/AUR ratios were maintained in a very low and narrow range (0.07-0.09). The
340 increased AURs (13.0-18.1 mg N/(g VSS·h)) were obtained when R ≤ 2 for both
341 applied aerated phase durations (3 or 5 min). The higher aeration on/off frequency

342 (aerated phase of 3 min) slightly increased the AOB activity without compromising the
343 NOB suppression. In general, the extended non-aerated phases resulted in the
344 decreased liquid N_2O concentrations and emission factors. However, further
345 increasing the R ratio (up to 3) negatively affected the AOB activity (AUR = 8.9-9.0 mg
346 N/(g VSS·h)) (scenarios 11 and 14).

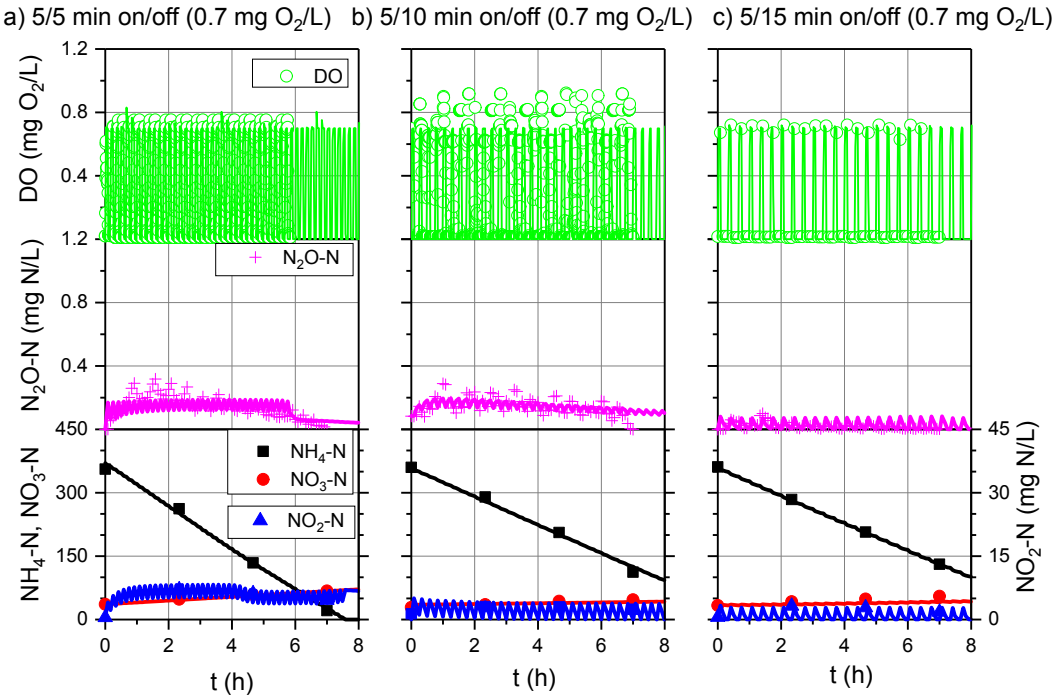

347

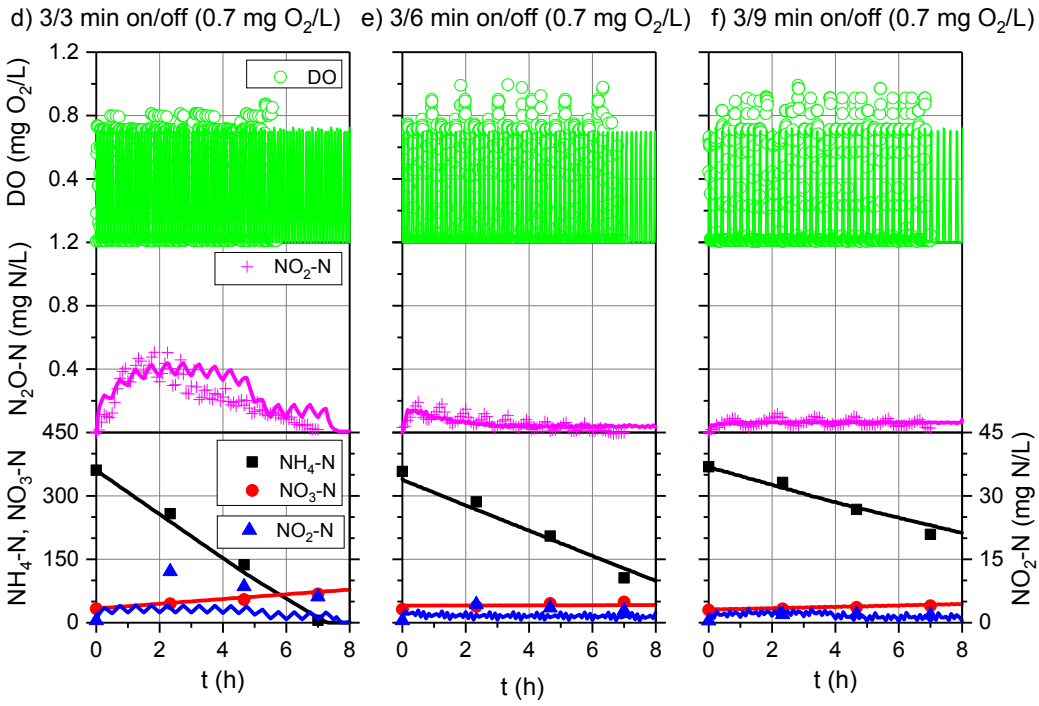

Figure 4. Measured data (scatters) vs. model predictions (solid lines) of DO and inorganic nitrogen compounds (N_2O-N, NH_4^+-N, NO_3^--N, NO_2^--N) in test trial no. 3: (a) intermittent aeration 5/5 min on/off at DO = 0.7 mg O_2/L (when on) (SCE9), (b) intermittent aeration 5/10 min on/off at DO = 0.7 mg O_2/L (when on) (SCE10), (c) intermittent aeration 5/15 min on/off at DO = 0.7 mg O_2/L (when on) (SCE11), (d) intermittent aeration 3/3 min on/off at DO = 0.7 mg O_2/L (when on) (SCE12), (e) intermittent aeration 3/6 min on/off at DO = 0.7 mg O_2/L (when on) (SCE13), (f) intermittent aeration 3/9 min on/off at DO = 0.7 mg O_2/L (when on) (SCE14).

The intermittent aeration pattern (8/22 min on/off at DO set point of 0.5 mg O_2/L in scenario 4), selected for the first stable operational period (5-154 d), was in accordance with the literature findings for deammonification systems [9,22,34]. In the stable operation period (158-308 d), the intermittent aeration pattern (5/20 min on/off

at DO = 0.7 mg O_2/L) was selected to avoid insufficient NOB inhibition or decline the AOB activity. The intermittent aeration pattern (3/6 min on/off at DO set point of 0.7 mg O_2/L in scenario 13) was ultimately selected to achieve the stable operation of the system in terms of NOB suppression and N_2O mitigation (Table S6). Experimental evidence of the efficient strategy was provided for a three-cycle simulation after reaching the stable phase-dynamic conditions in 20 days in order to evaluate the long-term efficiency of the selected strategy (Figure S3). The liquid N_2O concentrations were stable around 0.14 mg N/L while the NOB activity was effectively suppressed (NPR/AUR = 0.09).

Literature data suggested that the anoxic phase duration between 5 and 20 min could effectively delay the *Nitrospira*-NOB activity after the anoxic phase, regardless of the aerated phase duration [1,9]. However, other researches proposed that the minimum non-aerated phase duration of 15-20 min along with an aerated phase duration no longer than 5-15 min would be essential to outcompete NOB [19,32]. Furthermore, a higher aeration on/off frequency at low DO set points could efficiently suppress the NOB activity, while maintaining high overall nitrogen removal performance (70-80%) [8,9,22]. Although previous studies showed that low DO set points favored NOB suppression due to a higher oxygen affinity of AOB compared to NOB, recent studies suggested that the tight control of oxygen supply (durations and proportions of on/off periods) rather than the DO set point may be critical for NOB suppression. This can be attributed to a time lag of the NOB activity in adaption to

aerobic conditions and anammox bacteria outcompeting NOB for NO_2^--N in anoxic periods [7,35]. In the present study, it was found that an appropriate R ratio was more influential than strict durations of the aeration on/off periods. For the acclimated biomass (test trial no. 3), the optimal conditions were observed for R ≤ 2, while increasing the R ratio to 3 resulted in declining the AOB activity.

Integration of the N_2O production profiles during the aerated and non-aerated phases revealed that approximately 50% of N_2O was produced during the aerated phases, which was lower than the value (80%) reported by Blum et al. [11]. In comparison with the continuous aeration, when almost all N_2O production was emitted to the gas phase, approximately half of the produced N_2O was subsequently emitted to the gas phase under the intermittent aeration conditions. The estimated N_2O emission factors (Table S6) were within the range of literature data for deammonification systems. e.g. 0.4-4.6% in terms of TN removed [11,15,17,36,37]. The vast majority (approximately 98%) of N_2O was emitted during the aerated phases, which was also close to the value (96%) reported by Blum et al. [11]. Potential contributions of the specific biochemical pathways, including NH_2OH oxidation, autotrophic denitrification and heterotrophic denitrification, are discussed in Section 3.4.

3.2. Identification of the microbial community structure for setting the biomass composition in the model. The abundance and taxonomical affiliations of the particular physiological bacterial groups in the biomass samples, collected during the calibration (CAL), recalibration (REC) and validation (VAL) phases, are summarized in Table S5.

403 The dominant groups gradually shifted from heterotrophs to autotrophs (Figure 5)
404 along with a decreasing microbial biodiversity (Figure S4). Among 67 bacterial species
405 detected in the CAL sample, 44 were detected after 150 days of the cultivation period
406 (REC), and only 18 at the end of the experiment (VAL).

407

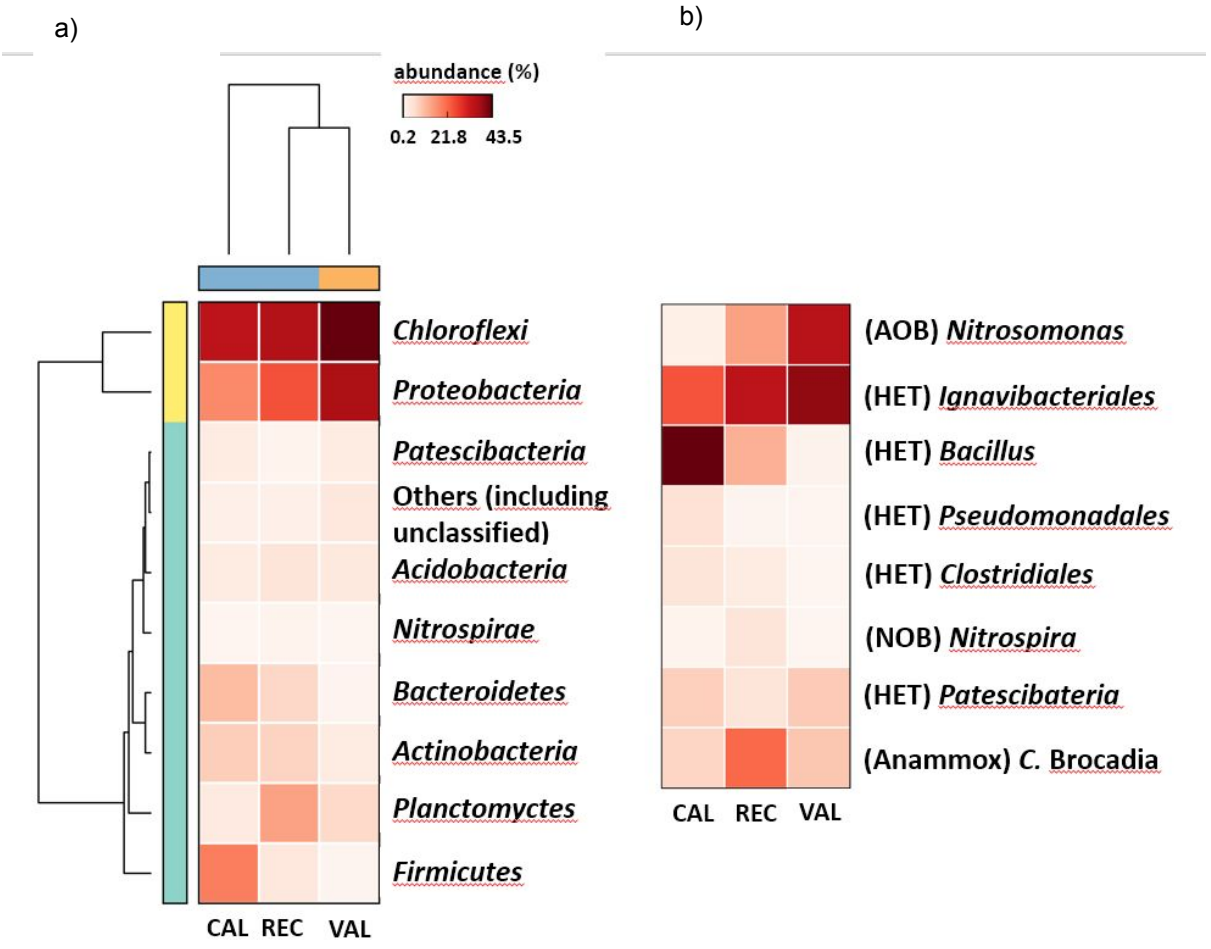

408

409 **Figure 5.** Heatmap of the differences between abundance of the bacterial phyla with
410 the genetic distance between the samples (upper dendrogram) and between taxa (left
411 dendrogram) (a) and representatives of the specific physiological bacteria groups (b)
412 in the CAL, REC and VAL samples (The term “Others” refers to the sum of all
413 classifications with less than 0.7% abundance and unclassified reads).

While microorganisms with the predominated heterotrophic metabolism decreased their abundance from 68.0% to 47.4%, the abundance of autotrophic bacterial groups explicitly tended to increase. The AOB were almost entirely represented by members of the genus *Nitrosomonas*, which constituted 0.7% of the overall bacterial community in the CAL sample. During the first 150 days of the cultivation period, their population increased to 2.7% (REC) and continued to grow up to 9.0% in the final stage of the experiment (VAL). This trend indicated a key role of r-strategist *Nitrosomonas* in ammonium oxidation in the studied SBR.

NOB were exclusively represented by the genus *Nitrospira* from the phylum *Nitrospirae*, which accounted for 0.2%, 0.7% and 0.1% in the CAL, REC and VAL samples, respectively. In terms of r/K theory with respect to nitrifiers, the selected dominant abundance of K-strategist *Nitrospira* could be attributed to two operational factors, including low DO and NO_2^--N concentrations as well as diffusion limitation within granules [38]. In comparison with the known NOB, comammox bacteria (complete ammonia oxidizers performing complete oxidation of ammonia to nitrate) were discovered from the genus *Nitrospira*. These bacteria could be favored at low temperature, low nitrogen substrate, and high DO conditions [39]. In the studied SBR, both AOB and NOB abundance increased during the cultivation period. Therefore, it is difficult to unambiguously determine if some *Nitrospira*-NOB indeed performed the metabolic comammox pathway, even though the potential was already reported in an anammox-enriched SBR [40].

The phylum *Planctomycetes*, which includes anammox bacteria, constituted 3.0% of the initial microbial population. However, only approximately 0.04% of DNA sequences from the total number of reads were assigned to the typical anammox bacteria from the genera *Candidatus* Brocadia. After first 150 days of the cultivation period, the bacteria belonging to the phylum *Planctomycetes* comprised 14.0%. *Candidatus* Brocadia related microorganisms reflected the dominant share of 8.7% in the REC sample, however, their share decreased to 2.4% at the end of the experiment (VAL sample).

3.3. Quantitative assessment of model calibration and validation. *3.3.1 Setting the initial model inputs for simulations.* The initial biomass composition (X_{HET}, X_{AOB}, X_{NOB}, X_{AMX}, X_S, $X_{U,}$ X_{EPS}) in the CAL, REC, and VAL phases was as follows: (i) 68%, 0.7%, 0.2%, 0.04%, 28.6%, 2.5%, 0% (ii) 42%, 2.7%, 0.7%, 8.7%, 42%, 3.7%, 0% and (iii) 47%, 9%, 0.1%, 2.4%, 38%, 3%, 0%, respectively. The microbial composition and biomass concentrations were used as microbial input to reduce the model uncertainty. The model kinetic parameter values, including the maximum specific growth rates and key saturation/inhibition coefficients, are listed in Table S4. The default values were adopted from literature and assumed based on the nitrogen conversion rates, microbial input, r/K strategist explanation and diffusional explanation.

3.3.2. Model calibration. In test trial no. 1, scenario 2 was first calibrated as a representative for the intermittent aeration pattern. 7 parameters were found very/extremely influential ($S_{i,j} \geq 1$) to NO_2^--N and N_2O-N, i.e. η_{gHET2}, η_{gHET3}, $K_{NO2,AOB}$,

456 $K_{O,AOB}$, $K_{O,NOB}$, K_h and η_h (Table S7). Parameter estimation showed a good
457 agreement between the observations and model predictions ($|r|_{N2O}$ > 0.8) (Table S8).
458 However, based on the correlation matrix (Figure S5a), three of them were found
459 highly cross-correlated with more than one parameter and thus they were excluded
460 from estimation. After the iterative parameter estimation (Tables S9-S10) along with
461 correlation analysis (Figure S5b-c), altogether 4 correlation crossing parameters (
462 η_{gHET3}, $K_{NO2,AOB}$, K_h and η_h) were excluded from the subset. The objective of the
463 iterative parameter estimation was to obtain the minimum number of identifiable
464 parameters (η_{gHET2}, $K_{O,AOB}$, $K_{O,NOB}$) that explain the data in scenario 2.

465 *3.3.3. Model recalibration.* Model recalibration was performed in scenario 6 to
466 achieve one unique parameter set for test trials no. 1-2. Based on the sensitivity
467 analysis for the prior parameter subset (Table S11), 2 previously excluded parameters
468 (η_{gHET3} and K_h) were added due to their very/extremely high influence ($S_{i,j}$ ≥ 1) to
469 NO_2^--N and N_2O-N in scenario 6. The expansion of the subset (η_{gHET2}, η_{gHET3}, $K_{O,AOB}$,
470 $K_{O,NOB}$, K_h) increased the goodness-of-fit for both scenario 2 ($|r|_{N2O}$ > 0.8) and scenario
471 6 ($|r|_{N2O}$ > 0.5), and no highly-correlated parameter pairs were found in the latter
472 scenario (Figure S5d). Finally, the mean value from both scenarios was determined
473 as the final value of the adjusted parameters (Table S12).

474 *3.3.4. Model validation.* Model validation was performed with the adjusted
475 parameters in the remaining scenarios in test trial no. 3. Table S13 shows evaluation
476 of the model accuracy using Pearson's $|r|$, root of mean squared errors (RMSE) and

Nash-Sutcliff coefficient (NSE) in all the scenarios. Pearson's $|r|_{N2O}$ varied in the range 0.69-0.94 (test trial no. 1), 0.34-0.73 (test trial no. 2) and 0.19-0.79 (test trial no. 3). Apart from 4 unsatisfactory goodness-of-fit results (scenarios 8, 10, 11, 14, $|r|_{N2O}$ < 0.5), the N_2O predictions accurately fitted the observations in the remaining scenarios. Generally, NH_4^+-N, NO_3^--N, NO_2^--N were predicted better than N_2O. The RMSE and NSE varied in the range 0.02-0.38 and -2.2-0.83 (except for the unsatisfactory goodness-of-fit performance of scenario 11), respectively. The higher R ratio allowed to decrease the liquid N_2O concentrations and the prediction accuracy decreased when the liquid N_2O concentrations were maintained at a low level, thus causing the unsatisfactory goodness-of-fit results. A comparison of RMSE and NSE with Pearson's $|r|$ revealed that they poorly correlated, implying the necessity of more than one criterion to improve the prediction accuracy. A global measure of model performance and model uncertainty is discussed elsewhere [31].

The adjusted parameters were η_{gHET2}, η_{gHET3}, $K_{O,AOB}$, $K_{O,NOB}$ and K_h (Table S12). The heterotrophic reduction factors for NO_2^--N and N_2O (η_{gHET2} = 0.17, η_{gHET3} = 0.40) and the hydrolysis rate (K_h = 2.6 d^{-1}) were within the literature range (η_{gHET2} = 0.016-0.3, η_{gHET3} = 0.075-0.81, K_h = 1.5-4.5 d^{-1}) [41,42]. The AOB oxygen affinity constant ($K_{O,AOB}$ = 0.10 mg O_2/L) was lower than that of NOB ($K_{O,NOB}$ = 0.52 mg O_2/L) and both values were typical for either r-strategist *Nitrosomonas*-AOB ($K_{O,AOB}$ = 0.03-1.22 mg O_2/L) or K-strategist *Nitrospira-NOB* ($K_{O,NOB}$ = 0.5-0.6 mg O_2/L) [43]. The relatively high oxygen affinity for K-strategist *Nitrospira* in comparison with r-strategist

498 *Nitrobacter* ($K_{O,NOB}$ = 0.43-1.1 mg O_2/L) [1] could also explain the difficulty of NOB
499 suppression under low DO conditions.

500 **3.4. Identification of the N_2O production pathways, NOB suppression mechanisms**
501 **and role of EPS.** The model predictions, shown in Figure 6a, suggest that the readily
502 biodegradable substrate (S_S), hydrolysed from the main biomass decay product (X_S),
503 was the main organic carbon source for heterotrophs. Both SMP components (UAP
504 and BAP) could hardly be utilized by heterotrophs due to the low generation rates of
505 SMP from biomass growth and low affinities of heterotrophs. The EPS pool tended to
506 accumulate thus decreasing the availability of organic carbon for the growth of
507 heterotrophs. As a consequence, the share of heterotrophic biomass decreased from
508 68% in the CAL phase to 42-47% in the REC/VAL phases. Such a model prediction is
509 consistent with the microbiological results, where representatives of *Anaerolineae*
510 from the *Chloroflexi* phylum increased their share from 25% (CAL) to 34% (VAL) in the
511 total bacterial community. That member of *Chloroflexi* is implicitly the microorganism
512 responsible for EPS production and plays an important role in the structural formation
513 of granules [44].

514 The finding of the present study is different from results of a theoretical modelling
515 study in an anammox biofilm system [28] which was validated based on earlier
516 experimental data [45]. The authors proposed that heterotrophs primarily grew on UAP
517 produced mainly from anammox growth. This difference, compared to the present
518 study, explicitly results from the major biomass components, including anammox

519 bacteria (60%) and EPS (20%), whereas the fraction of heterotrophs remained
520 relatively small (10%).

521 The model predictions revealed that NH_2OH oxidation (NN) and autotrophic
522 denitrification (ND) were the dominating pathways of N_2O production in the aerated
523 phase (80-100%) and non-aerated phase (60-90%), respectively. Heterotrophic
524 denitrification served as a sink for N_2O production under both aerated (20-30%) and
525 non-aerated phase (70-80%) (Figure 6b). For comparison, either NH_2OH oxidation or
526 autotrophic denitrification pathway has been reported as the dominant pathway in a
527 deammonification system under oxic conditions ($DO \geq 0.2$ mg O_2/L) and a wide range
528 of the influent NH_4^+-N and NO_2^--N concentrations [10]. Even though the heterotrophic
529 denitrification pathway has been neglected in most deammonification modelling studies,
530 Wan et al. [13] showed that heterotrophic denitrification could act as a sink in deeper
531 layers (anoxic condition) of deammonification granules even without organic carbon in
532 the influent feed.

533 The N_2O production rate was dependent on the AUR in the aerated phase and NO_2^--
534 N concentration in the non-aerated phase (Figure S6), which is similar to the findings
535 of Blum et al. [11]. Intense aeration could result in higher N_2O production and emission
536 due to both higher AURs and stripping effect, as suggested by Castro-Barros et al. [15],
537 and weaker suppression of the NOB activity (as shown in scenarios 2-3). A longer
538 non-aerated phase could cause more N_2O consumption by heterotrophic

539 denitrification, but it could also lead to lower AURs and NPR/AURs (as shown in
540 scenarios 5-8).

541 Ma et al. [19] attributed the mechanism of NOB suppression by intermittent aeration to
542 the periodic inhibition by FA (threshold of 0.2 mg N/L) corresponding to periodic pH
543 upshifts during the non-aerated phase. Higher aeration on/off frequencies could also
544 cause more often pH upshifts and enhance NOB suppression. However, in the present
545 study, the pH upshifts in relation to the intermittent aeration pattern were negligible as
546 the pH value was controlled in the range 7.5-7.9 by dosing NaOH. The consumption
547 of NH_4^+-N in the reaction phase resulted in the overall decrease in the FA
548 concentration in the range 1-9 mg N/L and 0-21 mg N/L in test trial no. 1 and test trials
549 no. 2-3, respectively. The FA inhibition thresholds were reported in the range 0.64-4.3
550 mg N/L for NOB [46,47], and specifically 0.04-0.08 mg N/L for *Nitrospira* [48]. Recent
551 studies have also shown contradictory results that FA concentrations in the range
552 18.1–25.0 mg N/L had a limited effect on NOB suppression [49], implicitly due to the
553 diverse NOB community. It should be noted that the different size of granules could
554 also have a potential effect on diffusion limitations and variations in the NOB activity.
555 However, this effect was not considered in the present study due to a relatively stable
556 granule size. In the present study, a similar FA decreasing trend under different R
557 ratios could not explain the stronger NOB suppression related to the longer non-
558 aerated phase. In addition, FNA inhibition on NOB was not considered because FNA
559 concentrations (< 0.002 mg N/L) were below the threshold values (0.02-0.1 mg N/L)

560 [46] during all the experiments. However, Blum et al. [12] suggested that pH may regulate
561 the rates between N_2O production and consumption. Indeed, Kanders et al. [50] showed
562 that more N_2O could be reduced via complete denitrification at higher pH (7.5-7.6 vs.
563 6.6-7.1). However, in the present study, such influence was avoided by controlling a
564 narrow pH range (7.5-7.9).

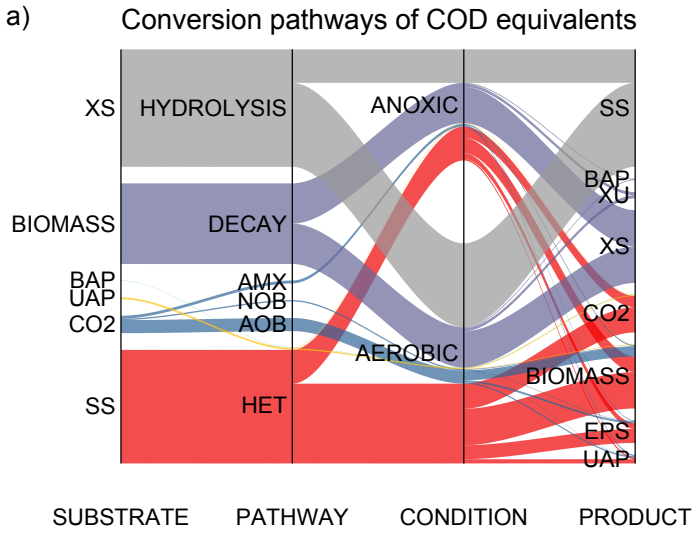

565

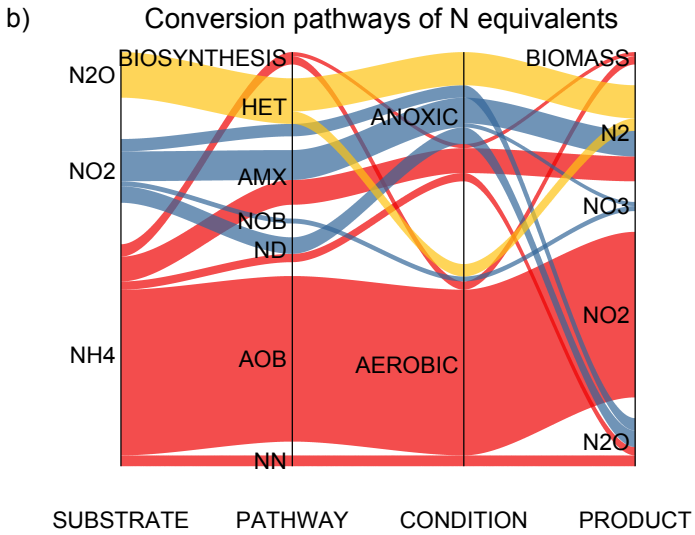

566

567 **Figure 6.** Sankey graph showing the conversion pathways of COD equivalents (a) and
568 N equivalents (b) at the end of the experimental period (based on the results of

scenario 13) (for higher sharpness, contributions smaller than 0.3% (a) and 1% (b) were neglected).

3.5. Model-based intermittent aeration strategies for performance optimization. The AOB activity, NOB activity and N_2O emissions, evaluated under different aeration strategies when the DO set point, R ratio and F frequency were respectively fixed to 0.7 mg O_2/L, 2 and 6.5 h^{-1}, are shown in Figure S7, whereas the remaing scenarios are shown in Figures S7-S9. The aeration strategies scattered in the red region were feasible only when the DO set point, R ratio and F frequency were within the range 0.5-2.1 mg O_2/L, 1.5-3.5 and 3-10 h^{-1}, respectively. At the reference state (DO=0.7 mg O_2/L, R=2 and F=6.5 h^{-1}), the predicted AUR, NPR/AUR and N_2O emission factor were approximately 12 mg N/(g VSS·h), 0.05 and 1%, respectively, which was close to the experimental findings (scenario 13) (13 mg N/(g VSS·h), 0.07 and 1% at DO=0.7 mg O_2/L, R=2 and F=6.5 h^{-1}). The AOB activity could be increased to 14 mg N/(g VSS·h) without compromising the NOB suppression (NPR/AUR < 0.1) and N_2O emission (E_{N2O} < 2%). This increase could result from either decreasing the R ratio to 1.5 (Figure S7a-c), or increasing the DO set point to 1.3 mg O_2/L (Figure S7d-f). The intermittent aeration with either higher DO set point and higher R ratio or lower DO set point and lower R ratio was suggested to maintain AUR > 12 mg N/(g VSS·h), NPR/AUR < 0.1 and E_{N2O} < 2% (Figure S7g-i).

As shown in Figures S7-S9, the R ratio and DO set point were crucial parameters for performance optimization, however, with the opposite effects on NOB suppression

590 and N_2O mitigation. The AOB activity could be slightly improved by either decreasing
591 the R ratio or increasing the DO set point. In the meantime, a higher F frequency was
592 suggested to maintain the sufficient NOB suppression and N_2O mitigation (Figures S8-
593 S9). Similar parabolic-shaped optimal range of the R ratio and DO set point were found
594 when the fixed F frequency exceeded 3 h^{-1} (Figure S10). The R ratio should tightly be
595 controlled when the DO set point was adjusted. Increasing the F frequency could further
596 expand the feasible region for both R ratio and DO set point.
597

598 ASSOCIATED CONTENT

599 **Supporting Information**.

600 The Supporting Information is available free of charge.

601 Experimental setup, model development, calibration and validation procedure,
602 definition of the state variables, stoichiometric matrix, kinetic rate equations, model
603 parameters, sensitivity analysis, correlation matrices and further metagenomics and
604 modelling results (PDF)

605 AUTHOR INFORMATION

606 **Corresponding Author**

607 *Tel.: +48 733811987; E-mail: xilu@pg.edu.pl

608 **Notes**

The authors declare no competing financial interest.

ACKNOWLEDGMENT

This study has been financially supported by the Polish National Center for Research and Development under the project “Reduction of N2O emissions from wastewater treatment plants - measurements, modeling and process optimization (RENEMO)” from Polish-German Cooperation for Sustainable Development Programme (WPN/7/2013), Major Science and Technology Program for Water Pollution Control and Treatment, China (2017ZX07206-002) and International Exchange Program for Graduate Students, Tongji University (No. 201801024).

REFERENCES

(1) Cao, Y.; van Loosdrecht, M. C. M.; Daigger, G. T. Mainstream Partial Nitritation–Anammox in Municipal Wastewater Treatment: Status, Bottlenecks, and Further Studies. *Appl. Microbiol. Biotechnol.* **2017**, *101* (4), 1365–1383. https://doi.org/10.1007/s00253-016-8058-7.

(2) Duan, H.; Ye, L.; Lu, X.; Yuan, Z. Overcoming Nitrite Oxidizing Bacteria Adaptation through Alternating Sludge Treatment with Free Nitrous Acid and Free Ammonia. *Environ. Sci. Technol.* **2019**, *53*, 1937–1946. https://doi.org/10.1021/acs.est.8b06148.

(3) Feng, Y.; Lu, X.; Al-Hazmi, H.; Mąkinia, J. An Overview of the Strategies for the Deammonification Process Start-up and Recovery after Accidental Operational Failures. *Rev. Environ. Sci. Biotechnol.* **2017**, *16* (3), 541–568. https://doi.org/10.1007/s11157-017-9441-2.

(4) Miao, Y.; Zhang, L.; Li, B.; Zhang, Q.; Wang, S.; Peng, Y. Enhancing Ammonium Oxidizing Bacteria Activity Was Key to Single-Stage Partial Nitrification-Anammox System Treating Low-Strength Sewage under Intermittent Aeration Condition. *Bioresour. Technol.* **2017**, *231*, 36–44. https://doi.org/10.1016/j.biortech.2017.01.045.

(5) Zhang, M.; Wang, S.; Ji, B.; Liu, Y. Towards Mainstream Deammonification of Municipal Wastewater: Partial Nitrification-Anammox versus Partial Denitrification-Anammox. *Sci. Total Environ.* **2019**, *692*, 393–401. https://doi.org/10.1016/j.scitotenv.2019.07.293.

(6) Noophan, P. L.; Figueroa, L. A.; Munakata-Marr, J. Nitrite Oxidation Inhibition by Hydroxylamine: Experimental and Model Evaluation. *Water Sci. Technol.* **2004**, *50* (6), 295–304. https://doi.org/10.2166/wst.2004.0388.

(7) Gao, H.; Scherson, Y. D.; Wells, G. F. Towards Energy Neutral Wastewater Treatment: Methodology and State of the Art. *Env. Sci Process. Impacts* **2014**, *16* (6), 1223–1246.

640 https://doi.org/10.1039/C4EM00069B.
641 (8) Han, M.; De Clippeleir, H.; Al-Omari, A.; Wett, B.; Vlaeminck, S. E.; Bott, C.; Murthy, S. Impact
642 of Carbon to Nitrogen Ratio and Aeration Regime on Mainstream Deammonification. *Water Sci.*
643 *Technol.* **2016**, *74* (2), 375–384. https://doi.org/10.2166/wst.2016.202.
644 (9) Miao, Y.; Zhang, L.; Yang, Y.; Peng, Y.; Li, B.; Wang, S.; Zhang, Q. Start-up of Single-Stage
645 Partial Nitrification-Anammox Process Treating Low-Strength Swage and Its Restoration from
646 Nitrate Accumulation. *Bioresour. Technol.* **2016**, *218*, 771–779.
647 https://doi.org/10.1016/j.biortech.2016.06.125.
648 (10) Ma, C.; Jensen, M. M.; Smets, B. F.; Thamdrup, B. Pathways and Controls of N2O Production
649 in Nitritation–Anammox Biomass. *Environ. Sci. Technol.* **2017**, *51* (16), 8981–8991.
650 https://doi.org/10.1021/acs.est.7b01225.
651 (11) Blum, J.-M.; Jensen, M. M.; Smets, B. F. Nitrous Oxide Production in Intermittently Aerated
652 Partial Nitritation-Anammox Reactor: Oxic N2O Production Dominates and Relates with
653 Ammonia Removal Rate. *Chem. Eng. J.* **2018**, *335*, 458–466.
654 https://doi.org/10.1016/j.cej.2017.10.146.
655 (12) Blum, J.-M.; Su, Q.; Ma, Y.; Valverde-Pérez, B.; Domingo-Félez, C.; Jensen, M. M.; Smets, B.
656 F. The PH Dependency of N-Converting Enzymatic Processes, Pathways and Microbes: Effect
657 on Net N_2O Production: PH Dependency of N-Converting Enzymatic Processes, Pathways and
658 Microbes. *Environ. Microbiol.* **2018**. https://doi.org/10.1111/1462-2920.14063.
659 (13) Wan, X.; Baeten, J. E.; Volcke, E. I. P. Effect of Operating Conditions on N2O Emissions from
660 One-Stage Partial Nitritation-Anammox Reactors. *Biochem. Eng. J.* **2019**, *143*, 24–33.
661 https://doi.org/10.1016/j.bej.2018.12.004.
662 (14) Massara, T. M.; Malamis, S.; Guisasola, A.; Baeza, J. A.; Noutsopoulos, C.; Katsou, E. A Review
663 on Nitrous Oxide (N2O) Emissions during Biological Nutrient Removal from Municipal
664 Wastewater and Sludge Reject Water. *Sci. Total Environ.* **2017**, *596–597*, 106–123.
665 https://doi.org/10.1016/j.scitotenv.2017.03.191.
666 (15) Castro-Barros, C. M.; Daelman, M. R. J.; Mampaey, K. E.; van Loosdrecht, M. C. M.; Volcke, E.
667 I. P. Effect of Aeration Regime on N2O Emission from Partial Nitritation-Anammox in a Full-
668 Scale Granular Sludge Reactor. *Water Res.* **2015**, *68*, 793–803.
669 https://doi.org/10.1016/j.watres.2014.10.056.
670 (16) Domingo-Félez, C.; Mutlu, A. G.; Jensen, M. M.; Smets, B. F. Aeration Strategies To Mitigate
671 Nitrous Oxide Emissions from Single-Stage Nitritation/Anammox Reactors. *Environ. Sci.*
672 *Technol.* **2014**, *48* (15), 8679–8687. https://doi.org/10.1021/es501819n.
673 (17) Leix, C.; Drewes, J. E.; Ye, L.; Koch, K. Strategies for Enhanced Deammonification Performance
674 and Reduced Nitrous Oxide Emissions. *Bioresour. Technol.* **2017**, *236*, 174–185.
675 https://doi.org/10.1016/j.biortech.2017.03.182.
676 (18) Corbalá-Robles, L.; Picioreanu, C.; van Loosdrecht, M. C. M.; Pérez, J. Analysing the Effects of
677 the Aeration Pattern and Residual Ammonium Concentration in a Partial Nitritation-Anammox
678 Process. *Environ. Technol.* **2016**, *37* (6), 694–702.
679 https://doi.org/10.1080/09593330.2015.1077895.
680 (19) Ma, Y.; Domingo-Félez, C.; Plósz, B. Gy.; Smets, B. F. Intermittent Aeration Suppresses Nitrite-
681 Oxidizing Bacteria in Membrane-Aerated Biofilms: A Model-Based Explanation. *Environ. Sci.*

Technol. **2017**, *51* (11), 6146–6155. https://doi.org/10.1021/acs.est.7b00463.

(20) Baeten, J. E.; Batstone, D. J.; Schraa, O. J.; van Loosdrecht, M. C. M.; Volcke, E. I. P. Modelling Anaerobic, Aerobic and Partial Nitritation-Anammox Granular Sludge Reactors - A Review. *Water Res.* **2019**, *149*, 322–341. https://doi.org/10.1016/j.watres.2018.11.026.

(21) Baeten, J. E.; van Loosdrecht, M. C. M.; Volcke, E. I. P. Modelling Aerobic Granular Sludge Reactors through Apparent Half-Saturation Coefficients. *Water Res.* **2018**, *146*, 134–145. https://doi.org/10.1016/j.watres.2018.09.025.

(22) Jardin, N.; Hennerkes, J. Full-Scale Experience with the Deammonification Process to Treat High Strength Sludge Water – a Case Study. *Water Sci. Technol.* **2012**, *65* (3), 447. https://doi.org/10.2166/wst.2012.867.

(23) Zaborowska, E.; Lu, X.; Makinia, J. Strategies for Mitigating Nitrous Oxide Production and Decreasing the Carbon Footprint of a Full-Scale Combined Nitrogen and Phosphorus Removal Activated Sludge System. *Water Res.* **2019**, *162*, 53–63. https://doi.org/10.1016/j.watres.2019.06.057.

(24) Klindworth, A.; Pruesse, E.; Schweer, T.; Peplies, J.; Quast, C.; Horn, M.; Glöckner, F. O. Evaluation of General 16S Ribosomal RNA Gene PCR Primers for Classical and Next-Generation Sequencing-Based Diversity Studies. *Nucleic Acids Res.* **2013**, *41* (1), 1–11. https://doi.org/10.1093/nar/gks808.

(25) Parks, D. H.; Beiko, R. G. Identifying Biologically Relevant Differences between Metagenomic Communities. *Bioinformatics* **2010**, *26* (6), 715–721. https://doi.org/10.1093/bioinformatics/btq041.

(26) Lu, X.; D. S. Pereira, T.; Al-Hazmi, H. E.; Majtacz, J.; Zhou, Q.; Xie, L.; Makinia, J. Model-Based Evaluation of N2O Production Pathways in the Anammox-Enriched Granular Sludge Cultivated in a Sequencing Batch Reactor. *Environ. Sci. Technol.* **2018**, *52* (5), 2800–2809. https://doi.org/10.1021/acs.est.7b05611.

(27) Azari, M.; Le, A. V.; Lübken, M.; Denecke, M. Model-Based Analysis of Microbial Consortia and Microbial Products in an Anammox Biofilm Reactor. *Water Sci. Technol.* **2018**, *77* (7), 1951–1959. https://doi.org/10.2166/wst.2018.081.

(28) Liu, Y.; Sun, J.; Peng, L.; Wang, D.; Dai, X.; Ni, B.-J. Assessment of Heterotrophic Growth Supported by Soluble Microbial Products in Anammox Biofilm Using Multidimensional Modeling. *Sci. Rep.* **2016**, *6* (1), 1–11. https://doi.org/10.1038/srep27576.

(29) Mozumder, Md. S. I.; Picioreanu, C.; van Loosdrecht, M. C. M.; Volcke, E. I. P. Effect of Heterotrophic Growth on Autotrophic Nitrogen Removal in a Granular Sludge Reactor. *Environ. Technol.* **2014**, *35* (8), 1027–1037. https://doi.org/10.1080/09593330.2013.859711.

(30) Henze, M.; Gujer, W.; Mino, T.; van Loosedrecht, M. *Activated Sludge Models ASM1, ASM2, ASM2d and ASM3*; IWA TASK GROUP ON MATHEMATICAL MODELLING FOR DESIGN AND OPERATION OF BIOLOGICAL WASTEWATER TREATMENT, Ed.; IWA Publishing: UK, 2000.

(31) Lu, X.; Al-Hazmi, H.; Majtacz, J.; Mannina, G.; Makinia, J. The Influence of the Objective Functions and a Priori Parameter Distribution on the Model Uncertainty of N2O Production in a Deammonification System. In *10th International Congress on Environmental Modelling and Software*; Brussels, Belgium, 2020.

(32) Gilbert, E. M.; Agrawal, S.; Brunner, F.; Schwartz, T.; Horn, H.; Lackner, S. Response of Different

724 Nitrospira Species To Anoxic Periods Depends on Operational DO. *Environ. Sci. Technol.* **2014**,
725 *48* (5), 2934–2941. https://doi.org/10.1021/es404992g.
726 (33) Sabba, F.; Terada, A.; Wells, G.; Smets, B. F.; Nerenberg, R. Nitrous Oxide Emissions from
727 Biofilm Processes for Wastewater Treatment. *Appl. Microbiol. Biotechnol.* **2018**, *102* (22), 9815–
728 9829. https://doi.org/10.1007/s00253-018-9332-7.
729 (34) Miao, Y.; Peng, Y.; Zhang, L.; Li, B.; Li, X.; Wu, L.; Wang, S. Partial Nitrification-Anammox (PNA)
730 Treating Sewage with Intermittent Aeration Mode: Effect of Influent C/N Ratios. *Chem. Eng. J.*
731 **2018**, *334*, 664–672. https://doi.org/10.1016/j.cej.2017.10.072.
732 (35) Ma, B.; Bao, P.; Wei, Y.; Zhu, G.; Yuan, Z.; Peng, Y. Suppressing Nitrite-Oxidizing Bacteria
733 Growth to Achieve Nitrogen Removal from Domestic Wastewater via Anammox Using
734 Intermittent Aeration with Low Dissolved Oxygen. *Sci. Rep.* **2015**, *5* (1), 1–9.
735 https://doi.org/10.1038/srep13048.
736 (36) Connan, R.; Dabert, P.; Moya-Espinosa, M.; Bridoux, G.; Béline, F.; Magrí, A. Coupling of Partial
737 Nitritation and Anammox in Two- and One-Stage Systems: Process Operation, N2O Emission
738 and Microbial Community. *J. Clean. Prod.* **2018**, *203*, 559–573.
739 https://doi.org/10.1016/j.jclepro.2018.08.258.
740 (37) Yang, J.; Trela, J.; Plaza, E. Nitrous Oxide Emissions from One-Step Partial Nitritation/Anammox
741 Processes. *Water Sci. Technol.* **2016**, *74* (12), 2870–2878. https://doi.org/10.2166/wst.2016.454.
742 (38) Arnaldos, M.; Amerlinck, Y.; Rehman, U.; Maere, T.; Van Hoey, S.; Naessens, W.; Nopens, I.
743 From the Affinity Constant to the Half-Saturation Index: Understanding Conventional Modeling
744 Concepts in Novel Wastewater Treatment Processes. *Water Res.* **2015**, *70*, 458–470.
745 https://doi.org/10.1016/j.watres.2014.11.046.
746 (39) Mehrani, M.-J.; Sobotka, D.; Kowal, P.; Ciesielski, S.; Makinia, J. The Occurrence and Role of
747 Nitrospira in Nitrogen Removal Systems. *Bioresour. Technol.* **2020**, *303*, 122936.
748 https://doi.org/10.1016/j.biortech.2020.122936.
749 (40) Ciesielski, S.; Czerwionka, K.; Sobotka, D.; Dulski, T.; Makinia, J. The Metagenomic Approach
750 to Characterization of the Microbial Community Shift during the Long-Term Cultivation of
751 Anammox-Enriched Granular Sludge. *J. Appl. Genet.* **2018**, *59* (1), 109–117.
752 https://doi.org/10.1007/s13353-017-0418-1.
753 (41) Mannina, G.; Cosenza, A.; Ekama, G. A. A Comprehensive Integrated Membrane Bioreactor
754 Model for Greenhouse Gas Emissions. *Chem. Eng. J.* **2018**, *334*, 1563–1572.
755 https://doi.org/10.1016/j.cej.2017.11.061.
756 (42) Pan, Y.; Ni, B.-J.; Lu, H.; Chandran, K.; Richardson, D.; Yuan, Z. Evaluating Two Concepts for
757 the Modelling of Intermediates Accumulation during Biological Denitrification in Wastewater
758 Treatment. *Water Res.* **2015**, *71*, 21–31. https://doi.org/10.1016/j.watres.2014.12.029.
759 (43) Park, M.-R.; Park, H.; Chandran, K. Molecular and Kinetic Characterization of Planktonic
760 *Nitrospira* Spp. Selectively Enriched from Activated Sludge. *Environ. Sci. Technol.* **2017**, *51* (5),
761 2720–2728. https://doi.org/10.1021/acs.est.6b05184.
762 (44) Speirs, L. B. M.; Rice, D. T. F.; Petrovski, S.; Seviour, R. J. The Phylogeny, Biodiversity, and
763 Ecology of the Chloroflexi in Activated Sludge. *Front. Microbiol.* **2019**, *10*, 2015.
764 https://doi.org/10.3389/fmicb.2019.02015.
765 (45) Ni, B.-J.; Ruscalleda, M.; Smets, B. F. Evaluation on the Microbial Interactions of Anaerobic

766 Ammonium Oxidizers and Heterotrophs in Anammox Biofilm. *Water Res.* **2012**, *46* (15), 4645–
767 4652. https://doi.org/10.1016/j.watres.2012.06.016.
768 (46) Park, S.; Bae, W. Modeling Kinetics of Ammonium Oxidation and Nitrite Oxidation under
769 Simultaneous Inhibition by Free Ammonia and Free Nitrous Acid. *Process Biochem.* **2009**, *44*
770 (6), 631–640. https://doi.org/10.1016/j.procbio.2009.02.002.
771 (47) Ushiki, N.; Jinno, M.; Fujitani, H.; Suenaga, T.; Terada, A.; Tsuneda, S. Nitrite Oxidation Kinetics
772 of Two Nitrospira Strains: The Quest for Competition and Ecological Niche Differentiation. *J.*
773 *Biosci. Bioeng.* **2017**, *123* (5), 581–589. https://doi.org/10.1016/j.jbiosc.2016.12.016.
774 (48) Blackburne, R.; Vadivelu, V. M.; Yuan, Z.; Keller, J. Kinetic Characterisation of an Enriched
775 Nitrospira Culture with Comparison to Nitrobacter. *Water Res.* **2007**, *41* (14), 3033–3042.
776 https://doi.org/10.1016/j.watres.2007.01.043.
777 (49) Zhang, F.; Yang, H.; Wang, J.; Liu, Z.; Guan, Q. Effect of Free Ammonia Inhibition on NOB
778 Activity in High Nitrifying Performance of Sludge. *RSC Adv.* **2018**, *8* (56), 31987–31995.
779 https://doi.org/10.1039/C8RA06198J.
780 (50) Kanders, L.; Yang, J.-J.; Baresel, C.; Zambrano, J. Full-Scale Comparison of N2O Emissions
781 from SBR N/DN Operation versus One-Stage Deammonification MBBR Treating Reject Water
782 – and Optimization with PH Set-Point. *Water Sci. Technol.* **2019**, *79* (8), 1616–1625.
783 https://doi.org/10.2166/wst.2019.163.

784 ABSTRACT ART.

785